

A Phonon Scattering Bottleneck for Carrier Cooling in Lead Chalcogenide Nanocrystals

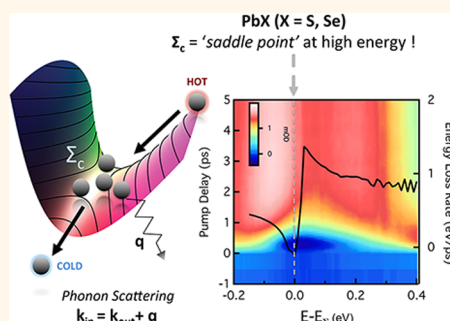
Pieter Geiregat,^{†,‡,§} Christophe Delerue,[‡] Yolanda Justo,^{‡,§} Michiel Aerts,^{||} Frank Spoor,^{||} Dries Van Thourhout,^{†,§} Laurens D. A. Siebbeles,^{||} Guy Allan,[‡] Arjan J. Houtepen,^{||,‡} and Zeger Hens^{*,‡}

[†]Photonics Research Group, Ghent University, 9000 Ghent, Belgium, [‡]Physics and Chemistry of Nanostructures, Ghent University, 9000 Ghent, Belgium,

[§]Center for Nano and Biophotonics, Ghent University, 9000 Ghent, Belgium, ^{||}IEMN, Département ISEN, UMR CNRS, 59046 Lille Cedex, France, and

^{||}Optoelectronic Materials Section, TU Delft, 2628 BL Delft, The Netherlands

ABSTRACT The cooling dynamics of hot charge carriers in colloidal lead chalcogenide nanocrystals is studied by hyperspectral transient absorption spectroscopy. We demonstrate a transient accumulation of charge carriers at a high energy critical point in the Brillouin zone. Using a theoretical study of the cooling rate in lead chalcogenides, we attribute this slowing down of charge carrier cooling to a phonon scattering bottleneck around this critical point. The relevance of this observation for the possible harvesting of the excess energy of hot carriers by schemes such as multiexciton generation is discussed.



KEYWORDS: PbS · PbSe · quantum dots · transient absorption spectroscopy · electron–phonon interaction · multiple exciton generation

Absorption of photons by a semiconductor with an energy exceeding the band gap transition results in the formation of hot electron–hole pairs that quickly dissipate their excess free energy, resulting in (quasi) thermalized conduction band electrons and valence band holes. For photovoltaic solar energy conversion, this cooling of the hot electron–hole pair is a major loss channel that restricts the maximum conversion efficiency of a single junction solar cell to the Shockley–Queisser limit.^{1,2} Harvesting this excess free energy by competing processes such as hot charge carrier transfer has proven challenging due to the high cooling rate, which can reach 1 ps^{-1} or more due to electron–phonon and/or carrier–carrier interactions.³ On the other hand, good use can be made of the high cooling rate for all-optical light modulation, where response times of a few ps have been demonstrated using, *e.g.*, hot carriers generated by light absorption in graphene⁴ or injected in ITO through a plasmonic nanoparticle as a sensitizer.⁵ Similar approaches of hot electron transfer following the optical excitation of surface

plasmons have recently been applied in catalysis,⁶ photovoltaics,⁷ photodetection⁷ and nanoscopic imaging.⁸

In the field of semiconductor nanocrystals or quantum dots (QDs), electron–hole pair cooling has attracted wide interest especially since a slowing down of electron and hole cooling due to a phonon bottleneck was predicted.⁹ The discrete energy levels in QDs may be separated by several LO phonon energies, hence requiring multiphonon emission for cooling, a process which is very unlikely. Whereas for specially designed QDs, a slowing of the cooling of the conduction band electron from its 1P to its 1S state could be confirmed,¹⁰ carrier cooling appeared to remain fast in most QDs with rates still close to 1 ps^{-1} , a result often attributed to additional cooling pathways involving Auger processes or energy transfer to surface ligands.¹⁰ Nevertheless, it proved possible to harvest the excess energy of hot excitons either by hot carrier transfer^{11,12} or the generation of multiple excitons.^{13–15} Both processes involve hot electron–hole pairs with a substantial excess energy, at least the QD band gap in the

* Address correspondence to zeger.hens@ugent.be.

Received for review November 3, 2014 and accepted January 7, 2015.

Published online January 07, 2015
10.1021/nn5062723

© 2015 American Chemical Society

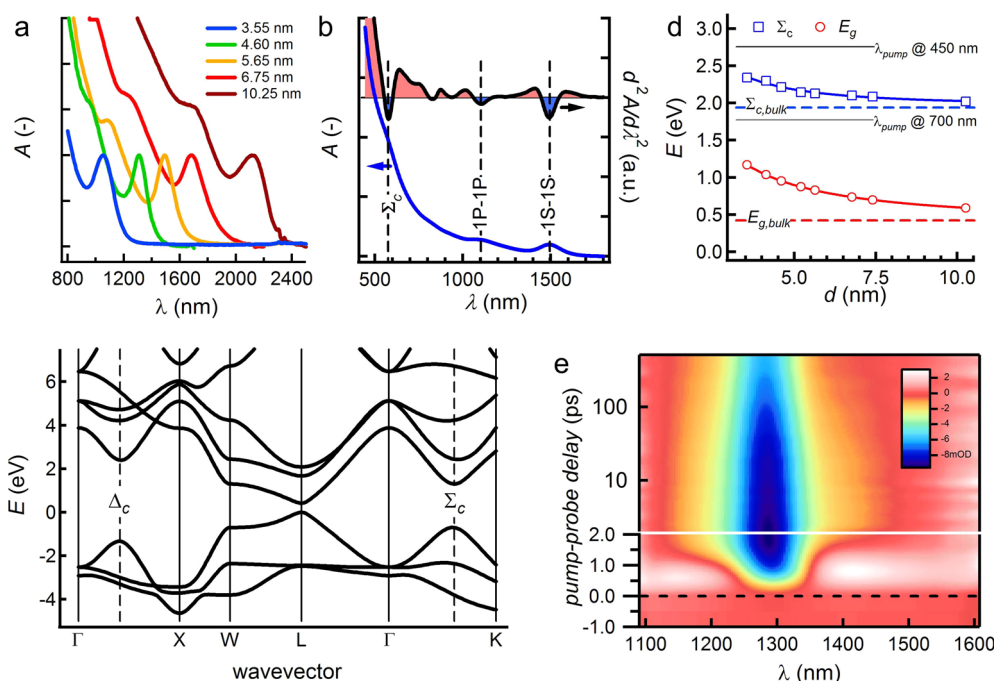


Figure 1. (a) Overview of absorption spectra of PbS QDs of different sizes, including (blue, orange, dark red) the three samples used in this study. For each spectrum, the legend indicates the average diameter as determined from the maximum of the first exciton absorption.²¹ (b) Absorption spectrum and second derivative spectrum of 5.65 nm PbS QDs with an assignment of the most relevant absorption features as the 1S–1S, 1P–1P and Σ_c transition. (c) Representation of the PbS bulk band structure with an indication of the critical points Σ_c and Δ_c along Σ and Δ . (d) Size-dependence of the 1S–1S and the Σ_c transition energy, together with an indication (dashed lines) of the corresponding bulk values²² and the photon energies corresponding to the pump wavelengths used in this study. (e) Time-wavelength map of the differential absorbance near the bandgap transition for 4.6 nm PbS nanocrystals.

case of multiple exciton generation, and their efficiency therefore depends on competition with cooling of electrons and holes occupying energy levels far from the band edges. Most studies of carrier cooling however focus on the changing occupation of states close to the band edge. Since filling of band-edge states is the end point of the cooling process, this only gives a view on the rate-determining step of the entire cooling cascade. This corresponds very often to the 1P–1S transition, which is the final stage of the cooling cascade. As a result, the thus obtained cooling rates may not be the most relevant for analyzing the competition between cooling and multiple exciton generation or hot carrier transfer.

Here, we analyze electron–hole pair cooling in PbS and PbSe colloidal QDs after excitation with high energy photons where, by means of white light transient absorption spectroscopy, energy levels throughout the entire Brillouin zone are probed. PbS and PbSe are probably the most widely studied QDs for photovoltaics and photodetection, showing effective multiple exciton generation at thresholds close to the theoretical limits^{13,14,16} and yielding the most efficient QD-based solar cells.¹⁷ In bulk, both have a direct band gap at the 4-fold degenerate L point of the Brillouin zone. At higher energy, there are a number of critical points, most notably along the Σ and Δ direction in the Brillouin zone, which add specific, size-dependent

features to the QD absorption spectrum.^{18–20} Most notably, we observe a transient accumulation of charge carriers at the critical point along the Σ direction, labeled as Σ_c , when the pump-photon energy exceeds the energy difference at Σ_c . We link this cooling bottleneck, which slows down carrier cooling to a net rate of $\approx 1 \text{ ps}^{-1}$ that is typically observed when monitoring band-edge states, to the energy level structure around Σ_c and we show that cooling *via* Σ_c is the dominant pathway for high energy charge carriers. Moreover, the buildup rate of the carrier population at Σ_c gives a direct way to probe cooling rates of high energy charge carriers, cooling rates that are most relevant for competing processes such as multiple exciton generation or hot carrier transfer.

EXPERIMENTAL RESULTS

Optical Properties of Lead-Chalcogenide Quantum Dots. We start with results obtained on PbS nanocrystal dispersions synthesized according to a procedure described by Moreels *et al.*,²³ with average diameters d_{NC} that we determined from the peak wavelength of the first exciton transition as indicated in Figure 1a.²¹ As shown in Figure 1b, various transitions between valence and conduction band states can be traced back by means of the second derivative of the absorbance, where next to the well-known 1S–1S and 1P–1P transitions a third transition at visible wavelengths stands out. In the case

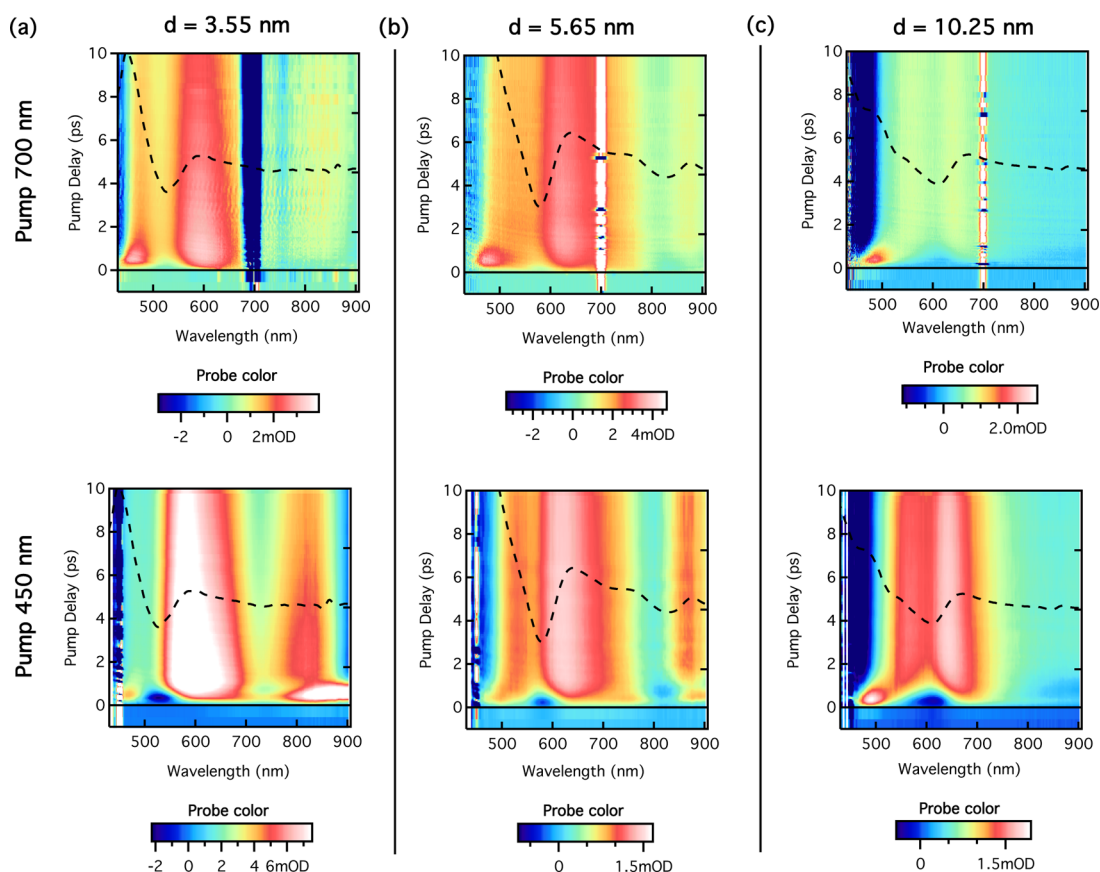


Figure 2. Contour maps of ΔA illustrating the carrier dynamics of the high energy transitions (*i.e.*, in the visible spectrum) for 3 different sizes of PbS quantum dots: (a) 3.55, (b) 5.65 and (c) 10.25 nm. Samples were pumped at 700 nm (top row) and 450 nm (bottom row). Color goes from negative (blue) to positive (red). The black dotted line is the second derivative of the corresponding linear absorption spectrum. The minimum corresponds to the onset of the absorption of the Σ -point transitions.

of PbSe QDs, a similar feature was attributed to electron transitions close to the critical point in the band structure along the Σ direction,²⁰ *i.e.*, the point we indicate as Σ_c (see Figure 1c). Figure 1d demonstrates that the feature appearing at visible wavelengths in the second derivative spectra of PbS QDs shows weaker confinement than the bandgap transition and extrapolates with increasing d_{NC} to the Σ_c energy difference of 1.94 eV as reported for bulk PbS.²² As this behavior is highly similar to that of the Σ_c transition in PbSe QDs, we also attribute this visible feature in PbS QDs to the electronic transitions around Σ_c as already suggested by Cadmeratari *et al.*¹⁹

Figure 1e shows the change of the absorption spectrum of 4.6 nm PbS QDs around their bandgap transition following a 180 fs laser pulse at 700 nm that creates on average 0.3 excitons per QD. The change in absorption, defined as the difference in absorbance $\Delta A = A^* - A_0$ of the dispersion after and before photoexcitation, respectively, is represented by a color code as a function of probe wavelength and time delay after the excitation pulse. The figure shows the typical reduction of the bandgap absorption due to the occupation of the band-edge states by photogenerated electrons and holes.²⁴ The buildup of the bleach

signal around the bandgap transition within the first 1–2 ps after the pump pulse reflects the final step of the cooling of the photogenerated charge carriers to the band-edge states, a process accompanied by a strong reduction of the sub-bandgap photoinduced absorption related to intraband transitions.²⁵

Above Band Gap Transient Absorption Spectroscopy. Being the result of a cascade of cooling steps *via* phonon emission, the rate of band-edge state filling may not give an accurate view on the initial cooling dynamics of the high energy electron and hole created by the pump pulse, which is the most relevant in view of competing processes such as hot carrier extraction or carrier multiplication.¹⁶ Therefore, we probed the transient absorption at photon energies well above the QD bandgap. As shown in Figure 2a–c, such above bandgap transient absorption maps are dominated by photoinduced absorption ($\Delta A > 0$) for all PbS QDs studied when using a pump wavelength of 700 nm ($\hbar\omega = 1.77$ eV). As outlined in the Supporting Information (section S1), this photoinduced absorption results from a spectral redshift that is largely independent of the probe wavelength. Following the argumentation developed in ref 26, we attribute this spectral shift to the net Coulomb interaction between

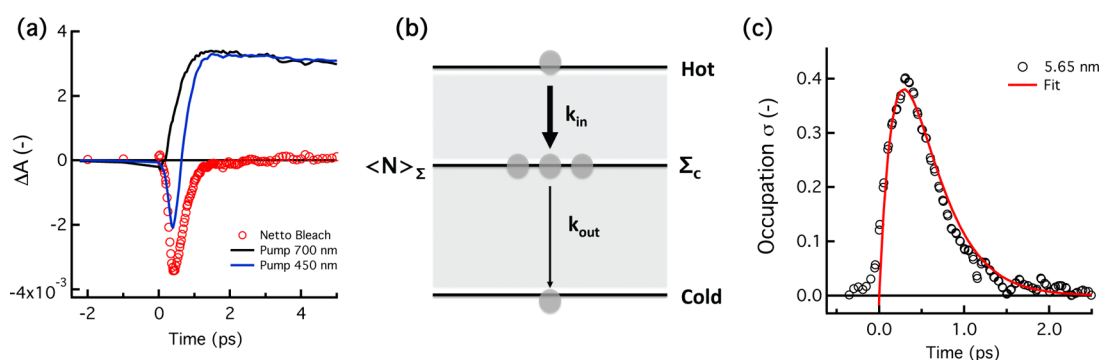


Figure 3. Kinetic analysis of ΔA of 5.65 nm QDs. (a) Carrier dynamics at Σ_c for excitation below (700 nm, solid black) and above (450 nm, solid blue) the Σ_c -transition. Empty markers indicate the netto bleach. (b) Schematic depicting simple 3-level approach to model the observed netto bleach at Σ_c : inflow from carriers from higher energy (hot) and outflow to lower energy (cold) levels. (c) Probability $\sigma(t)$ to have 1 exciton in the ensemble of Σ -states as a function of time (see text) for the 5.65 nm size PbS QDs. A fit to eq 1 of the experimental data (empty circles) is shown (solid red line).

the exciton(s) resulting from the pump-pulse and the exciton newly created by the probe pulse.

When changing the excitation wavelength to 450 nm, *i.e.*, to photon energy well above the Σ_c transition, the most notable difference in the transient absorption maps is the appearance of a short-lived negative ΔA at around 500–600 nm. A similar negative feature was observed by Cho *et al.*, who used degenerate pump–probe spectroscopy.²⁷ The occurrence of this bleach feature in the first 1–2 ps after photoexcitation, *i.e.*, the typical cooling time, points to the temporal blocking of electronic transitions due to the accumulation of cooling charge carriers in particular electronic states. The dashed line added to each transient absorption map in Figure 2 represents the second derivative of the respective absorption spectra, where the dip corresponds to the position of the Σ_c transition (see Figure 1b). It can be clearly seen that for each QD sample analyzed the wavelength range of the transient bleach corresponds to that of the Σ_c transition. We thus conclude that the cooling of charge carriers can be shortly delayed in the electronic states around the critical point along the Σ direction in the Brillouin zone. As outlined in the Supporting Information (section S2), a similar feature is observed in the case of PbSe QDs pumped at photon energies above the Σ_c transition.

Transient Bleach Kinetics at Σ_c . Taking vertical cuts through the 2D maps of Figure 2 at the maximum of this transient bleach feature, we obtain the kinetic traces displayed in Figure 3 for the 3.55 nm PbS nanocrystals. We clearly observe that excitation above the Σ_c -transition (at 450 nm pump) leads to a trace distinctly different from excitation below Σ_c (at 700 nm). While pumping at 700 nm only leads to the rapid buildup of a photoinduced absorption, a bleach feature develops and vanishes for the sample pumped at 450 nm on a subpicosecond time scale. If we interpret the transient absorption at 450 nm as composed of a bleach feature due to charge carrier

TABLE 1. Summary of the Rates of Cooling toward (k_{in}) and Away from (k_{out}) Σ_c as Obtained by Fitting the Experimental Traces to eq 1 and the Energy Loss Rate $w_{E,in}$ as Obtained from the Product of k_{in} and the Energy Per Charge Carrier to Be Dissipated for Cooling toward Σ_c

QD	d_{NC} (nm)	k_{in} (ps^{-1})	k_{out} (ps^{-1})	$w_{E,in}$ (eV ps^{-1})	$w_{ph,in}$ (ps^{-1})
PbS	3.55	3.8	2.8	0.76	29
PbS	5.65	3.9	2.9	1.2	45
PbS	10.2	4.1	3.1	1.5	58
PbSe	4.80	1.85	2.7	0.37	44

accumulation and photoinduced absorption due to exciton–exciton interaction, the trace recorded with a 700 nm pump can be seen as a measure for the photoinduced absorption background. The resulting net bleach, obtained by subtracting the (properly rescaled) 700 nm from the 450 nm pump trace has been added to Figure 3a.

We tentatively model this net bleach by considering 3 different states, representing hot carriers, carriers occupying states around Σ_c and cold carriers, where hot carriers occupy the states around Σ_c at a rate k_{in} and these cool down further at a rate k_{out} (see Figure 3b). As a result, the transient exciton population $\langle N \rangle_{\Sigma}(t)$ around Σ_c can be described as

$$\langle N \rangle_{\Sigma}(t) = \frac{k_{in}}{k_{out} - k_{in}} f \langle N \rangle (e^{-k_{in}t} - e^{-k_{out}t}) \quad (1)$$

Here, $\langle N \rangle$ represents the average number of excitons created per QD by the pump pulse and f is the fraction of excitons cooling *via* Σ_c . A fit of the net bleach to eq 1 is shown in Figure 3c, where the bleach signal has been rescaled to represent the occupation probability $\sigma(t)$ of the states around Σ_c ($\sigma(t) = \langle N \rangle_{\Sigma} / \langle N \rangle$). The corresponding rates k_{in} and k_{out} have been summarized in Table 1 for the different PbS QDs studied. One sees that, regardless of the QD size, the rate of cooling toward and away from Σ_c amounts to ≈ 3.8 and 2.8 ps^{-1} , which implies that $\sigma(t)$ reaches a maximum

value of ≈ 0.4 . We see that passage *via* the Σ direction critical point delays the cooling of charge carriers. By means of k_{in} , the 3-level model analysis provides a way to estimate the initial cooling rate of hot charge carriers and not the final cooling rates which are typically measured when looking at state filling of the band-edge states. Clearly, this initial cooling rate is what matters for most process aiming at harvesting the hot exciton energy. Moreover, this rate will also set a limit to applications such as light modulation that could make use of the rapid change of optoelectronic properties that come with cooling. It should be noted that the figure of $\approx 4 \text{ ps}^{-1}$ reported here most likely underestimates the cooling rate since it approaches the reciprocal of the temporal width of the pump pulse. Even so, we find that the cooling rate for high excess energy electron–hole pairs in PbSe QDs is significantly lower than for PbS QDs.

Transient Bleach Intensity at Σ_c . A key quantity in eq 1 is the fraction f of the excited electron–hole pairs that cool *via* Σ_c . When $f \approx 1$, most charge carriers experience a temporal slowing down of their cooling, which increases the probability for competing processes to harvest the excess free energy of the electron–hole pair. On the other hand, when $f \ll 1$, the observation of a slowdown of the cooling rate merely serves as a way to estimate the initial hot carrier cooling rate yet has little influence on the overall carrier cooling rate. Considering again the valence- and conduction-band states around Σ_c as single levels with respective degeneracies g_V and g_C provides us with a way to estimate f from the maximum bleach of the absorbance. Within this picture, the integrated absorption coefficient (related to the experimentally accessible absorbance A through $A = \alpha L / \ln 10$, with L the cuvette length) of the Σ_c transition can be written as

$$\alpha_{int, \Sigma_c} = g_V g_C \alpha_{0, \Sigma_c} \quad (2)$$

Here, α_{0, Σ_c} represents the average integrated absorption coefficient of an individual transition between valence and conduction band contributing to the Σ_c absorbance. If an exciton is present in these levels, the absorption coefficient changes due to state filling and the possibility for stimulated emission. The resulting nonlinear absorption coefficient reads

$$\alpha_{int, \Sigma_c}^* = (g_V - 1)(g_C - 1)\alpha_{0, \Sigma_c} - \alpha_{0, \Sigma_c} \quad (3)$$

As a result, we can write the normalized change in transmission (bleach) for an average occupation $\langle N \rangle$ as

$$\frac{\Delta \alpha}{\alpha_{int, \Sigma_c}} = \frac{\alpha_{int, \Sigma_c}^* - \alpha_{int, \Sigma_c}}{\alpha_{int, \Sigma_c}} = \frac{g_V + g_C}{g_V g_C} \langle N \rangle_{\Sigma_c} \quad (4)$$

Hence, the maximum normalized bleach after integration becomes

$$\frac{\Delta \alpha}{\alpha_{int, \Sigma_c}} = \frac{g_V + g_C}{g_V g_C} f \sigma_{\max} \langle N \rangle \quad (5)$$

To determine the fraction f of hot carriers cooling *via* Σ_c from the experimental transient absorption data, the degeneracies g_V and g_C must be known. Since there are 12 equivalent Σ directions, the degeneracies g_V and g_C should be 24 at least (including spin). On the other hand, g_V and g_C will be capped by the product of the density of states around Σ_c for bulk PbS and the spectral width of the Σ_c bleach. In Figure 4, we plot the density of states needed according to eq 5 to have $f = 1$ or $f = 0.1$ together with the above-mentioned lower and upper limits to the degeneracy, where we used a density of states of 0.5 eV/PbS unit cell for bulk PbS around Σ_c .²⁸ One sees that for all QD sizes studied, the degeneracy needed to have $f = 1$ closely agrees with that calculated from the bulk density of states while for the smallest QDs, $f = 0.1$ corresponds to degeneracies that are physically impossible. We thus conclude that a sizable fraction of the excitons, if not all excitons, cool *via* Σ_c and thus experience a transient slow-down of the cooling rate.

THEORETICAL ANALYSIS

Energy Band Structure of Bulk PbS. To gain a better understanding of the observed reduction of the cooling rate, we return to the band structure of bulk PbS, which we calculated within the tight-binding approximation. As shown in Figure 1c, the lowest conduction band minima and the highest valence band maxima are located at the 8-fold degenerate L points of the Brillouin zone. Other critical points can be found, for example, along the Σ ([110]) and Δ ([100]) direction, where in particular around Σ_c , our results point toward a slowing down of charge carrier cooling. Importantly, both Σ_c and Δ_c are saddle points, meaning that the first derivatives of the energy $E_{\mathbf{k}}$ with respect to the three components of \mathbf{k} vanishes, giving rise to a high density of states and a marked feature in the optical absorption spectrum, whereas the band curvature is either positive or negative depending on the direction in the Brillouin zone. For example, near $\mathbf{k}_{\Sigma_c} = (\pi/a)[1, 1, 0]$, the conduction band can be approximated as

$$E_{c, \mathbf{k}} \approx E_{c, \Sigma_c} + \frac{\hbar^2}{2} \left(\frac{\delta k_{110}^2}{m_{110}} + \frac{\delta k_{1\bar{1}0}^2}{m_{1\bar{1}0}} - \frac{\delta k_{001}^2}{m_{001}} \right) \quad (6)$$

Here, $\delta \mathbf{k} = (\delta k_{110}, \delta k_{1\bar{1}0}, \delta k_{001})$ is defined as the difference between the wavevector \mathbf{k} of the actual electron state and \mathbf{k}_{Σ_c} projected on the directions indicated by the subscript (see Figure 5a) and m_{110} ($0.20 m_0$), $m_{1\bar{1}0}$ ($0.17 m_0$) and m_{001} ($0.80 m_0$) are the corresponding effective masses. As shown in Figure 5b, the energy dispersion is positive along the [110] ($\Sigma_c \rightarrow K$) and $[1\bar{1}0]$ ($\Sigma_c \rightarrow X$) direction yet it is negative along [001] ($\Sigma_c \rightarrow L$) (these directions have been indicated in Figure 5a). Moreover, the effective mass is much larger, *i.e.*, the energy surface is far less curved, along [001] than along the two others directions, which feature similar

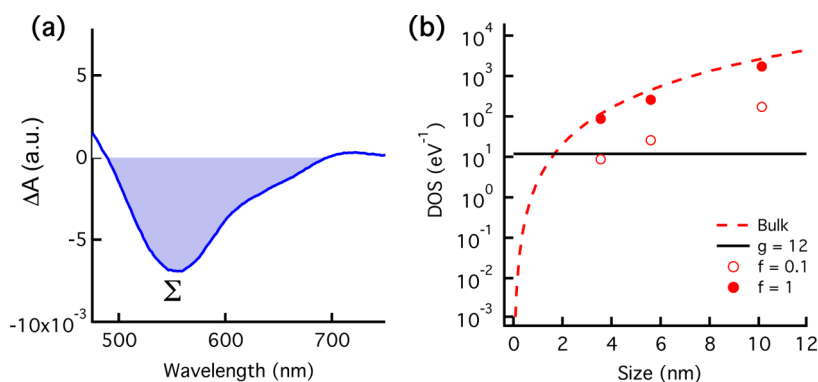


Figure 4. Estimation of fraction f of hot carriers cooling via Σ_c . (a) Netto bleach spectrum used to calculate the integrated absorption spectrum $\delta\alpha$. (b) Bulk prediction and lower limit for number of states involved in the Σ_c transition. Markers indicate the experimentally obtained values for $f = 0.1$ (empty markers) and $f = 1$ (filled markers). The coincidence of the $f = 1$ markers with the bulk number of states indicates that f is of the order of unity, indicating that also the fraction of the hot carriers cooling via Σ_c is of the order of unity.

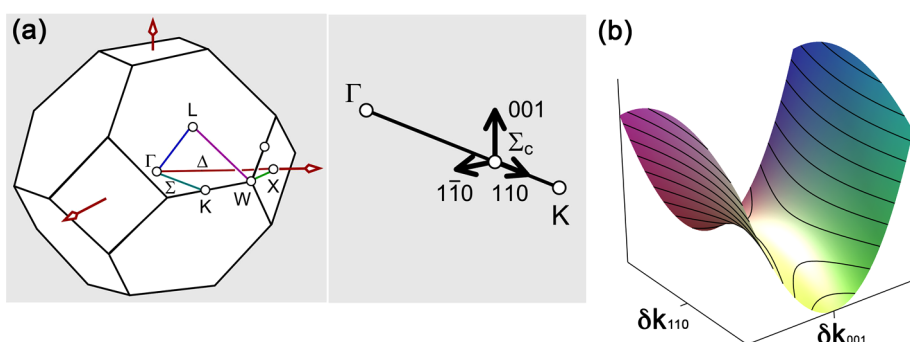


Figure 5. (a) Representation of (left) the Brillouin zone of the fcc lattice with an indication of the most prominent symmetry points and directions and (right) the local coordinate system introduced to analyze the dispersion relation around Σ_c . (b) 2D plot of the energy dispersion as a function of δk_{110} and δk_{001} showing pronounced positive curvature (light effective mass) along (110) and a relatively small negative curvature (heavy effective mass) along (001).

curvature. As discussed in the Supporting Information (section S3), this behavior can be traced back to the Pb–S $pp\sigma$ interaction dominating the formation of energy bands in PbS. As a result, a similar situation featuring an even more pronounced difference in effective masses exists for the valence band (see Supporting Information, section S3).

Carrier Cooling in Bulk PbS. The cooling of hot carriers in polar materials like PbS and PbSe is mainly due to scattering by longitudinal optical (LO) phonons,²⁹ where the matrix element describing the coupling between electrons and LO phonons has been derived by Fröhlich.^{30,31} Assuming dispersionless LO phonons of energy $\hbar\omega_{LO}$ (26 meV in PbS,³² 17 meV in PbSe³³), we accordingly define the rate of energy loss w_E as $\pm\hbar\omega_{LO}$ multiplied by the scattering rate w (in 1/s) for emission (+) or absorption (–) of a phonon. Using the Fermi golden rule, the energy loss rate for a carrier in a state $|\mathbf{k}\rangle$ can then be determined by summing over all possible phonon wavevectors \mathbf{q} :³⁰

$$w_E(\mathbf{k}) = \frac{(2\pi e\hbar\omega_{LO})^2}{\hbar V} \left(\frac{1}{\varepsilon(\infty)} - \frac{1}{\varepsilon(0)} \right) \sum_{\mathbf{q}} \frac{|\langle \mathbf{k} - \mathbf{q} | e^{-iq \cdot \mathbf{r}} | \mathbf{k} \rangle|^2}{q^2} \times \dots \\ \{ (N+1)\delta(E_{\mathbf{k}-\mathbf{q}} - E_{\mathbf{k}} + \hbar\omega_{LO}) - N\delta(E_{\mathbf{k}-\mathbf{q}} - E_{\mathbf{k}} - \hbar\omega_{LO}) \} \quad (7)$$

Here, $N = 1/[\exp(\hbar\omega_{LO}/kT) - 1]$ is the average number of phonons at temperature T in a given mode, ε_0 and ε_∞ are the static and high frequency dielectric constant and V is the crystal volume. The first term in the second line of eq 7 describes the emission of phonons, the second the absorption.

We used eq 7 to calculate the energy loss rate for hot charge carriers using the bulk PbS electron states calculated in tight-binding (see Methods section), considering 10^9 different \mathbf{q} vectors in the Brillouin zone. Both intra- and interband processes are considered, yet the dependence on $1/q^2$ in eq 7 implies that polar scattering has a much greater role in intraband than in interband processes.²⁹ Figure 6 represents the resulting rate at 300 K for electrons and holes near Σ_c . For electrons with a relatively high excess energy relative to E_{Σ_c} ($E - E_{\Sigma_c} \gg \hbar\omega_L$) the rate is more or less constant, in the eV ps^{-1} range. This is a typical result for hot carrier relaxation in polar materials²⁹ and its order of magnitude agrees with the rate $w_{E,\text{in}}$ derived here for carrier cooling toward Σ_c (see Table 1). However, when the carrier energy is progressively reduced, the rate first slightly increases but then suddenly drops, within an energy range more narrow than $\hbar\omega_L$, to reach very small, even negative values. Decreasing the energy below

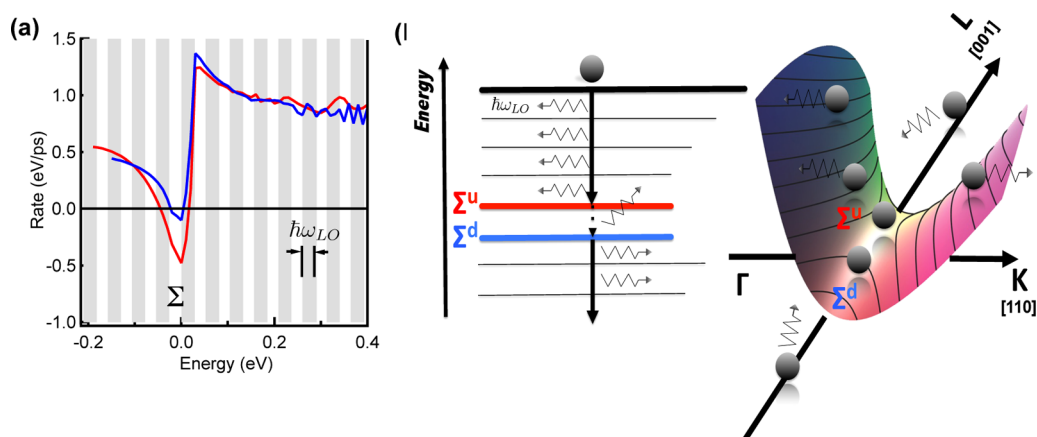


Figure 6. (a) Energy loss rate at 300K calculated for an electron (solid blue line) (hole, solid red line) placed in the lowest (highest) conduction (valence) band near the Σ_c ($k_0 = \pi/a[110]$) point where the zero of energy corresponds to the energy of Σ_c . The wavevector of the initial electron state is oriented along [110] with respect to k_0 for $E > 0$ and along [001] for $E < 0$ (b) A depiction of a hot carrier cooling through a process of fast phonon emission (with quantized energy $\hbar\omega_{LO}$) until a bottleneck transition is reached, denoted as $\Sigma_c^u \rightarrow \Sigma_c^d$.

E_{Σ_c} results again in a saturation of the cooling rate, yet at a smaller value than at high energy. The behavior for holes near Σ_c is similar, but even more pronounced. Negative rates are predicted in an energy window of about 70 meV at 300 K, which means that the hole has a higher probability to move up, *i.e.*, absorb a photon, than down. This is a direct consequence of the almost flat valence-band energy surface in the [001] direction, which implies a very high hole effective mass in that direction (see Supporting Information, section S3).

These findings can be understood more qualitatively by returning to eq 7, which shows that two elements favor high loss rates. First, nonzero contributions to the loss rate are only obtained for those phonons where the phonon energy and momentum matches the energy difference between the initial and a final electron state. Hence for a given phonon dispersion relation, the larger the electron density of states, the higher the cooling rate. Second, having $q^2 = |\mathbf{q}|^2$ in the numerator implies that high loss rates result from electron scattering by phonons that meet energy and momentum conservation with small magnitude phonon or scattering wavevectors \mathbf{q} , *i.e.*, when the gradient $\nabla_{\mathbf{k}}E$ is large (see Supporting Information, section S4). Returning to the dispersion relation around Σ_c , it follows that both elements favor rapid cooling toward Σ_c yet hamper cooling away from Σ_c . While there are two directions of positive curvature with low effective masses, there is only one of negative curvature with a high effective mass. This results in a higher density of states and steeper energy gradients above than below Σ_c , which makes that the change of direction of the scattering wavevector necessary to pass Σ_c constitutes a significant bottleneck for cooling of electrons and holes toward the band edges (see Supporting Information, section S4).

On the basis of the picture of preferential cooling of electrons along $-\nabla_{\mathbf{k}}E$, *i.e.*, the direction of steepest

descent, it may seem surprising that a sizable fraction of the charge carriers experience a slowing of their cooling rate. Indeed, since the conduction band energy dispersion around Σ_c corresponds to a hyperbolic paraboloid, with two directions of high positive curvature and one of low, negative curvature, only charge carriers created at the principle axes with positive curvature will cool toward Σ_c . However, the strong difference in curvature makes the conduction band energy dispersion resemble a gutter (see Figure 5b), where the direction of steepest descent will be almost perpendicular to the direction of negative curvature also for points off the two principle axes with positive curvature. As a result, also carriers created at these points will be forced to change direction abruptly when reaching the axis of negative curvature, which brings about the above-discussed slowing down of their cooling rate. Hence, even if the fraction of electrons and holes that exactly pass Σ_c during cooling may be small, a far larger number will be slowed down during cooling at energies close to that of Σ_c .

Importantly, Figure 6 shows that the energy range of slow cooling around Σ_c is one to two phonon energies wide. This results in a picture of high energy carriers that (1) cool toward Σ_c by the rapid, successive emission of LO phonons, (2) slow down around Σ_c due to the reorientation of the scattering wavevector, which involves one or two slow phonon emission steps and (3) continue cooling toward the band edge states by rapid, successive phonon emission. As discussed in the Supporting Information (section S5), this leads to a more precise interpretation of the rates k_{in} and k_{out} in the phenomenological 3-level model we introduced to describe the transient bleach around Σ_c . The incoming rate k_{in} is the effective rate of the first part of the cooling process. As such, it is equal to the ratio between the energy loss rate w_E and the energy the electron and the hole dissipate before reaching Σ_c or,

phrased differently, to the product of the phonon emission rate $w_{\text{ph},\text{in}}$ and the number of phonons to be emitted before reaching Σ_c . Both $w_{E,\text{in}}$ and $w_{\text{ph},\text{in}}$ thus calculated have been added to Table 1. Importantly, since the measured cooling rate k_{in} is close to the width of the pump pulse, the highest rates calculated should be seen as lower limits to the true energy loss and phonon emission rate. The outgoing rate k_{out} on the other hand corresponds to the slow emission of one or two phonons around Σ_c . Especially the comparison of the phonon emission rate for cooling toward ($w_{\text{ph},\text{in}} > 50 \text{ ps}^{-1}$) and around Σ_c ($w_{\text{ph},\text{out}} \approx 2.5\text{--}5 \text{ ps}^{-1}$) makes clear how considerable a bottleneck Σ_c is for carrier cooling.

From Bulk to Quantum Dots. Electron states in nanocrystals can be seen as linear combinations of bulk states, which essentially results in a quantization of the electron wavevectors \mathbf{k} . Taking the case of cubic nanocrystals with an edge length L for example, the energies E of the quantized states around Σ_c read

$$E = E_{c,\Sigma_c} + \frac{\hbar^2}{2m_{110}} \left(\frac{n_{110}\pi}{L} \right)^2 + \frac{\hbar^2}{2m_{1\bar{1}0}} \left(\frac{n_{1\bar{1}0}\pi}{L} \right)^2 - \frac{\hbar^2}{2m_{001}} \left(\frac{n_{001}\pi}{L} \right)^2 \quad (8)$$

Here, n_{110} , $n_{1\bar{1}0}$ and n_{001} are nonzero, positive integers that quantize the incremental wavevector $\delta\mathbf{k}$ in the directions indicated by the subscript. The experiments presented here show that at energies well above Σ_c , the cooling of hot carriers remains as efficient as in bulk, with very similar characteristic energy loss rates in the eV ps^{-1} range. We thus conclude that size quantization does not really limit the cooling of carriers in these energy ranges. Since the energy splitting between states is in practice never exactly equal to a LO phonon energy, multiphonon processes are required. The stronger coupling to acoustic phonons in nanocrystals compared to bulk certainly contributes to compensate the energy mismatch.^{34,35} However, the driving force for the relaxation remains the coupling to LO phonons which follows the same rules as in the bulk but taking into account quantized components.

In particular, it appears that all the conclusions about the dimensionality of the parameter space for the final state and the directionality of \mathbf{q} with respect to \mathbf{k} remain valid. In bulk, the threshold for the change in energy loss rate, linked to the necessary change in the direction of the scattering wavevector is near the energy gap ΔE_{Σ_c} at Σ_c . Given the difference in effective masses for the directions of positive and negative curvature, the threshold will be close to $\Delta E_{\Sigma_c} + \hbar^2\pi^2/L^2((1/m_{110}) + (1/m_{1\bar{1}0}))$ in nanocrystals. Further cooling requires an increase of the quantum number n_{001} , *i.e.*, the quantized equivalent of a change in direction of the scattering wavevector. Hence, we indeed expect the slow down of carrier cooling to shift to higher

energy for smaller nanocrystals and follow, as observed, the quantization of energy levels around Σ_c . eq 8 is only an approximation due to its dependence on a parabolic band structure and a particular nanocrystal geometry. More elaborate calculations show that the eigenstates are somewhat spread in \mathbf{k} space. In addition, since there are 12 Σ_c points, intervalley couplings mix all the states. Including the spin degree of freedom, this leads to a high density of states in the vicinity of Σ_c . These effects should contribute to broaden the energy range where the carrier accumulation occurs. However, the experimental results show that the underlying effects originating from the saddle points of the bulk remain efficient.

Cooling Around Other Saddle Points. The band structure of bulk PbS (PbSe) is characterized by other saddle points where a similar analysis could be applied to assess their influence on the cooling rate. Most notably, a saddle point Δ_c is present along the Δ direction ($\Gamma \rightarrow X$), whose energy gap of $\approx 3 \text{ eV}$ falls outside of the range of the TA setup used here. Calling this direction the parallel one, the band dispersion around $\mathbf{k}_{\Delta_c} \approx 0.82(\pi/a)(1,0,0)$ can be approximated as

$$E_{c,k} \approx E_{c,\Delta_c} + \frac{\hbar^2}{2} \left(\frac{\delta k_{\parallel}^2}{m_{\parallel}} - \frac{\delta k_{\perp}^2}{m_{\perp}} \right) \quad (9)$$

Here, we introduce the effective masses m_{\parallel} ($\approx 0.16m_0$) along Δ and m_{\perp} ($\approx 0.51m_0$) for the two directions perpendicular to Δ . In contrast to Σ_c , we calculate a strong enhancement of the cooling rate near Δ_c (see Supporting Information S6). This can be readily understood from the band dispersion where now two directions instead of one have a negative dispersion instead of one. Therefore, when the carrier is close to the saddle point, the parameter space for the final state is determined by one additional degree of freedom that considerably increases the density of allowed processes and thus the cooling rate. We thus predict that, opposite from Σ_c , Δ_c does not constitute a bottleneck for electron cooling.

DISCUSSION

The relaxation rate of hot electron–hole pairs is of particular importance for QD-based photovoltaic cells that exploit multiple-exciton generation (MEG), where a single hot electron–hole pair creates multiple electron–hole pairs with lower energy.^{15,40} Several authors have proposed that the efficiency of MEG is determined by the competition between the generation of multiple excitons *via* impact ionization and hot carrier relaxation.^{16,40–42} Therefore, the characterization of hot carrier relaxation is of great importance for understanding this MEG efficiency. The relevant rate in this context is the cooling rate of carriers at high excess energy, above the energy threshold for MEG E_{th} . In this respect, the results shown here raise the question as to

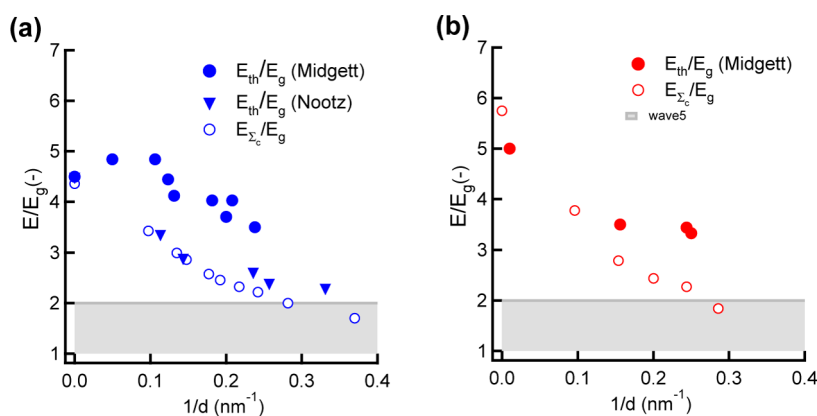


Figure 7. Comparison of Σ_c and threshold energy for MEG (normalized to the band gap energy E_g) for (a) PbS from Midgett³⁶ and Nootz³⁷ and (b) PbSe³⁸ as a function of the inverse particle size $1/d$. Note that the bulk limit³⁹ corresponds to $1/d = 0$.

whether the cooling bottleneck around Σ_c is responsible for the efficient MEG that is observed in PbS and PbSe QDs.

If indeed the occurrence of MEG is linked to slow cooling around Σ_c , one would expect the MEG threshold, *i.e.*, the energy where the yield of excitons starts to exceed 100%, to be related to E_{Σ_c} . Figure 7 therefore represents both E_{Σ_c} and the few available data on the MEG threshold for PbS^{36,37} and PbSe³⁶ QDs^{36,38,39} as a function of the reciprocal QD diameter $1/d_{NC}$, where the bulk values are also included at $1/d_{NC} = 0$.³⁹ In the case of bulk PbS and PbSe, E_{Σ_c}/E_g amounts to 4.36 and 5.75, respectively. Interestingly, both numbers correspond closely to the experimental bulk MEG thresholds as reported by Pijpers *et al.*³⁹ As a result of the higher effective masses at Σ_c compared to the band edge effective masses, E_{Σ_c}/E_g decreases with decreasing diameter. For both PbS and PbSe QDs, the MEG threshold follows the same trend, yet the available sets of data show considerable discrepancies. Whereas the MEG threshold as determined by Nootz *et al.* closely follows Σ_c ,³⁷ Midgett *et al.* report MEG thresholds that exceed E_{Σ_c}/E_g by more than the QD bandgap for 4 nm PbS and PbSe QDs. Figure 7 also indicates that for PbS and PbSe QDs smaller than ≈ 3.5 nm, E_{Σ_c}/E_g drops below 2. This is below the energy conservation threshold, which implies that the slow cooling around Σ_c is irrelevant for MEG observed in these QDs.

Since MEG by impact ionization is a process that competes with charge carrier cooling, the MEG efficiency in PbS and PbSe QDs is closely related to the cooling rate, where higher MEG efficiencies imply slower cooling.^{41–43} Focusing on PbS QDs, we have estimated the MEG efficiencies assuming that hot carrier relaxation results from this competition (see Supporting Information S7). Following the methodology described in ref 44, we have calculated the energy-dependent impact ionization rates in bulk PbS and PbS QDs. The phonon cooling is considered as a parameter independent of the carrier energy. Figure S10 shows that we theoretically retrieve MEG

efficiencies that closely follow E_{Σ_c}/E_g , as reported by Nootz *et al.*, for phonon emission rates of $\approx 2 \text{ ps}^{-1}$. On the other hand, we obtain the lower efficiencies found by Midgett *et al.* if the phonon emission rate is raised to $\approx 25 \text{ ps}^{-1}$. Based on the figures provided in Table 1, it follows that both possibilities can be consistent with our experimental data. If the MEG threshold effectively follows E_{Σ_c}/E_g , it requires a slowing down of the cooling to a rate that corresponds to what we find around Σ_c . On the other hand, if MEG is only effective for excitations well above E_{Σ_c} , it competes with a much faster cooling where again, the rate we measure can reasonably account for the experimental thresholds. It thus appears that the understanding of the mechanism behind MEG, and the possible role of the slow cooling around Σ_c requires a more precise determination of the MEG threshold as a function of QD size. Moreover, any theoretical model attempting to describe the MEG efficiency should start from the experimental results on hot charge carrier cooling presented in this manuscript, *i.e.*, cooling by phonon emission at rates of $\approx 50 \text{ ps}^{-1}$ (or more) for electron (hole) states above (below) Σ_c and at rates of the order of k_{out} around Σ_c .

CONCLUSION

In summary, we have shown that PbS and PbSe quantum dots exhibit a transient absorption bleach at photon energies corresponding to the Σ_c transition. This is interpreted in terms of a temporal accumulation of charge carriers due to a slowing down of charge carrier cooling. This temporal accumulation of cooling carriers enables us to quantify the energy loss rate of hot electron–hole pairs and to estimate that the fraction of hot carriers cooling *via* this Σ_c bottleneck is of the order of 1. Importantly, we demonstrate that this cooling bottleneck is intrinsically linked to the properties of the band structure of bulk PbS and PbSe around the critical point Σ_c . This indicates that cooling bottlenecks at critical points in the band structure present a general opportunity to

use hot charge carriers more efficiently. In this respect, an intriguing, very recent finding is that critical

points can be created on purpose in twisted bilayer graphene.⁴⁵

METHODS

Materials. Oleylamine (OLA) capped PbS quantum dots (QDs) were synthesized using the procedure described by Cademartiri *et al.*¹⁹ and modified by Moreels *et al.*²³ After synthesis, the (oleylamine) OLA ligand shell is substituted by oleic acid (OA). An exchange to OA is typically performed by adding OA to a toluene suspension of PbS Qdots in a ratio of 1.5:10 OA/toluene. After precipitation with ethanol and centrifugation, the QDs are resuspended in toluene and the exchange is repeated.

White Light Pump—Probe Spectroscopy. We present a hyperspectral analysis of the hot carrier decay in lead chalcogenide nanocrystals (NCs) using broadband and nondegenerate pump—probe spectroscopy. As such, 180 fs pulses are generated in a YKGBW oscillator (Light Conversion, Pharos SP) at 1028 nm and amplified. The majority of this fundamental beam is used to generate pump light at 450 and 700 nm using an OPA and second harmonics module (Light Conversion, Orpheus). A small fraction of the fundamental beam is split off to generate broadband 'white' light in a sapphire crystal. The probe light is delayed using an automated delay stage to achieve probe delays up to 3 ns. The colloidal NCs are diluted in tetrachloroethylene to achieve optical densities of 1 at the shortest excitation wavelength of 450 nm.

The fluence is chosen sufficiently low ($\langle N \rangle = J_{\text{ph}} \times \sigma_a \approx 0.1$) such that, at most, single excitons are present. Assuming a Poissonian distribution of the carrier population after photoexcitation, the probability P_N to have N excitations in one NC is given by

$$P_N = \frac{e^{-\langle N \rangle} \langle N \rangle^N}{N!} \quad (10)$$

Here, $\langle N \rangle$ is determined from $\langle N \rangle = J \times \sigma_{\text{pump}}$, where J is the pump fluence in photons/second and σ_{pump} is the photon absorption cross section at the pump wavelength λ_{pump} . We make sure $P_2 < 0.01$.

Conflict of Interest: The authors declare no competing financial interest.

Acknowledgment. The authors acknowledge Ghent University (BOF scholarship, GOA Detavernier-Hens), the FWO-Vlaanderen (G.0760.12), BelSPo (IAP 7.35, photonics@be), EU-FP7 (Strep Navolchi), FOM and ADEM.

Supporting Information Available: Information on the spectral shifts, the four-level approximation, the valence band dispersion around Σ_c , scatter rates and the analysis of the Δ_c critical point. Data for carrier cooling in PbSe nanocrystals is also provided. This material is available free of charge via the Internet at <http://pubs.acs.org>.

REFERENCES AND NOTES

- Shockley, W.; Queisser, H. Detailed Balance Limit of Efficiency of p—n Junction Solar Cells. *J. Appl. Phys.* **1961**, *32*, 510–519.
- Ross, R.; Nozik, A. Efficiency of Hot-Carrier Solar Energy Converters. *J. Appl. Phys.* **1982**, *53*, 3813–3818.
- Kambhampati, P. Hot Exciton Relaxation Dynamics in Semiconductor Quantum Dots: Radiationless Transitions on the Nanoscale. *J. Phys. Chem. C* **2011**, *115*, 22089–22109.
- Li, W.; Chen, B.; Meng, C.; Fang, W.; Xiao, Y.; Li, X.; Hu, Z.; Xu, Y.; Tong, L.; Wang, H.; *et al.* Ultrafast All-Optical Graphene Modulator. *Nano Lett.* **2014**, *14*, 955–959.
- Abb, M.; Albella, P.; Aizpurua, J.; Muskens, O. L. All-Optical Control of a Single Plasmonic Nanoantenna-ITO Hybrid. *Nano Lett.* **2011**, *11*, 2457–2463.
- Mukherjee, S.; Libisch, F.; Large, N.; Neumann, O.; Brown, L. V.; Cheng, J.; Lassiter, J. B.; Carter, E. A.; Nordlander, P.; Halas, N. J. Hot Electrons Do the Impossible: Plasmon-Induced Dissociation of H₂ on Au. *Nano Lett.* **2013**, *13*, 240–247.
- Clavero, C. Plasmon-induced Hot-Electron Generation at Nanoparticle/Metal-oxide Interfaces for Photovoltaic and Photocatalytic Devices. *Nat. Photonics* **2014**, *8*, 95–103.
- Giugni, A.; Torre, B.; Toma, A.; Francardi, M.; Malerba, M.; Alabastri, A.; Proietti Zaccaria, R.; Stockman, M. I.; Di Fabrizio, E. Hot-Electron Nanoscopy Using Adiabatic Compression of Surface Plasmons. *Nat. Nanotechnol.* **2013**, *8*, 845–852.
- Nozik, A. Spectroscopy and Hot Electron Relaxation Dynamics in Semiconductor Quantum Wells and Quantum Dots. *Annu. Rev. Phys. Chem.* **2001**, *52*, 193–231.
- Pandey, A.; Guyot-Sionnest, P. Slow Electron Cooling in Colloidal Quantum Dots. *Science* **2008**, *322*, 929–932.
- Tisdale, W. A.; Williams, K. J.; Timp, B. A.; Norris, D. J.; Aydil, E. S.; Zhu, X.-Y. Hot-Electron Transfer from Semiconductor Nanocrystals. *Science* **2010**, *328*, 1543–1547.
- Wang, H.; Barceló, I.; Lana-Villarreal, T.; Gómez, R.; Bonn, M.; Cánovas, E. Interplay Between Structure, Stoichiometry, and Electron Transfer Dynamics in SILAR-based Quantum Dot-Sensitized Oxides. *Nano Lett.* **2014**, *14*, 5780–5786.
- Sandeep, C. S. S.; Cate, S. T.; Schins, J. M.; Savenije, T. J.; Liu, Y.; Law, M.; Kinge, S.; Houtepen, A. J.; Siebbeles, L. D. A. High Charge-Carrier Mobility Enables Exploitation of Carrier Multiplication in Quantum-Dot Films. *Nat. Commun.* **2013**, *4*, 2360.
- Aerts, M.; Suchand Sandeep, C. S.; Gao, Y.; Savenije, T. J.; Schins, J. M.; Houtepen, A. J.; Kinge, S. S.; Siebbeles, L. D. A. Free Charges Produced by Carrier Multiplication in Strongly-Coupled PbSe Quantum Dot Films. *Nano Lett.* **2011**, *11*, 4485–4489.
- Semonin, O. E.; Luther, J. M.; Choi, S.; Chen, H.-Y.; Gao, J.; Nozik, A. J.; Beard, M. C. Peak External Photocurrent Quantum Efficiency Exceeding 100% via MEG in a Quantum Dot Solar Cell. *Science* **2011**, *334*, 1530–1533.
- Klimov, V. I.; Stewart, J. T.; Padilha, L. A.; Qazilbash, M.; Pietryga, J. M.; Midgett, A. G.; Luther, J.; Beard, M. C.; Nozik, A. Comparison of Carrier Multiplication Yields in PbS and PbSe Nanocrystals: The Role of Competing Energy-Loss Processes. *Nano Lett.* **2012**, *12*, 622–628.
- Lee, J.-W.; Son, D.-Y.; Ahn, T. K.; Shin, H.-W.; Kim, I. Y.; Hwang, S.-J.; Ko, M. J.; Sul, S.; Han, H.; Park, N.-G. Quantum-Dot-Sensitized Solar Cell with Unprecedentedly High Photocurrent. *Sci. Rep.* **2013**, *3*, 1050.
- Hens, Z.; Vanmaekelbergh, D.; Kooij, E.; Wormeester, H.; Allan, G.; Delerue, C. Effect of Quantum Confinement on the Dielectric Function of PbSe. *Phys. Rev. Lett.* **2004**, *92*, 026808.
- Cademartiri, L.; Montanari, E.; Calestani, G.; Migliori, A.; Guagliardi, A.; Ozin, G. A. Size-Dependent Extinction Coefficients of PbS Quantum Dots. *J. Am. Chem. Soc.* **2006**, *128*, 10337–10346.
- Koole, R.; Allan, G.; Delerue, C.; Meijerink, A.; Vanmaekelbergh, D.; Houtepen, A. J. Optical Investigation of Quantum Confinement in PbSe Nanocrystals at Different Points in the Brillouin Zone. *Small* **2008**, *4*, 127–133.
- Moreels, I.; Lambert, K.; Smeets, D.; De Muynck, D.; Nollet, T.; Martins, J. C.; Vanhaecke, F.; Vantomme, A.; Delerue, C.; Allan, G.; *et al.* Size-Dependent Optical Properties of Colloidal PbS Quantum Dots. *ACS Nano* **2009**, *3*, 3023–3030.
- Kanazawa, H.; Adachi, S. Optical Properties of PbS. *J. Appl. Phys.* **1998**, *83*, 5997–6001.
- Moreels, I.; Justo, Y.; De Geyter, B.; Hastraete, K.; Martins, J. C.; Hens, Z. Size-tunable, Bright, and Stable PbS

- Quantum Dots: A Surface Chemistry Study. *ACS Nano* **2011**, *5*, 2004–2012.
24. Klimov, V. Optical Nonlinearities and Ultrafast Carrier Dynamics in Semiconductor Nanocrystals. *J. Phys. Chem. B* **2000**, *104*, 6112–6123.
 25. De Geyter, B.; Houtepen, A. J.; Carrillo, S.; Geiregat, P.; Gao, Y.; Ten Cate, S.; Schins, J. M.; Van Thourhout, D.; Delerue, C.; Siebbeles, L. D.; *et al.* Broadband and Picosecond Intra-band Absorption in Lead-Based Colloidal Quantum Dots. *ACS Nano* **2012**, *6*, 6067–6074.
 26. Geiregat, P.; Houtepen, A.; Justo, Y.; Grozema, F. C.; Van Thourhout, D.; Hens, Z. Coulomb Shifts upon Exciton Addition to Photoexcited PbS Colloidal Quantum Dots. *J. Phys. Chem. C* **2014**, *118*, 22284–22290.
 27. Cho, B.; Peters, W. K.; Hill, R. J.; Courtney, T. L.; Jonas, D. M. Bulklike Hot Carrier Dynamics in Lead Sulfide Quantum Dots. *Nano Lett.* **2010**, *10*, 2498–2505.
 28. Kohn, S.; Yu, P.; Petroff, Y.; Shen, Y.; Tsang, Y.; Cohen, M. Electronic Band Structure and Optical Properties of PbTe, PbSe and PbS. *Phys. Rev. B: Condens. Matter Mater. Phys.* **1973**, *8*, 1477–1488.
 29. Conwell, E. In *High Field Transport in Semiconductors*; Turnbull, D., Ehrenreich, H., Eds.; Academic Press: New York, NY, 1967.
 30. Fröhlich, H.; Pelzer, H.; Zienau, S. Properties of Slow Electrons in Polar Materials. *Philos. Mag.* **1950**, *41*, 221–242.
 31. Fröhlich, H. Theory of Electrical Breakdown in Ionic Crystals. *Proc. R. Soc. London, Ser. A* **1937**, *160*, 230–241.
 32. Dalven, R. Electron-Optical-Polaron Coupling Constant in PbS, PbSe and PbTe. *Phys. Rev. B: Condens. Matter Mater. Phys.* **1971**, *3*, 1953–1954.
 33. Habinshuti, J.; Kilian, O.; Cristini-Robbe, O.; Sashchiuk, A.; Addad, A.; Turrell, S.; Lifshitz, E.; Grandier, B.; Wirtz, L. Anomalous Quantum Confinement of the Longitudinal Optical Phonon Mode in PbSe Quantum Dots. *Phys. Rev. B: Condens. Matter Mater. Phys.* **2013**, *88*, 115313.
 34. Kohn, W.; Luttinger, J. Motion of Electrons and Holes in Perturbed Periodic Fields. *Phys. Rev.* **1955**, *97*, 869–883.
 35. Takagahara, T. Electron-Phonon Interactions and Excitonic Dephasing in Semiconductor Nanocrystals. *Phys. Rev. Lett.* **1993**, *71*, 3577–3580.
 36. Midgett, A. G.; Luther, J. M.; Stewart, J. T.; Smith, D. K.; Padilha, L. A.; Klimov, V. I.; Nozik, A. J.; Beard, M. C. Size and Composition Dependent Multiple Exciton Generation Efficiency in PbS, PbSe, and PbS_xSe_{1-x} Alloyed Quantum Dots. *Nano Lett.* **2013**, *13*, 3078–3085.
 37. Nootz, G.; Padilha, L.; Levina, L.; Sukhovatkin, V.; Webster, S.; Brzozowski, L.; Sargent, E.; Hagan, D.; Van Stryland, E. Size Dependence of Carrier Dynamics and Carrier Multiplication in PbS Quantum Dots. *Phys. Rev. B: Condens. Matter Mater. Phys.* **2011**, *83*, 155302.
 38. Midgett, A. G.; Hillhouse, H. W.; Hughes, B. K.; Nozik, A. J.; Beard, M. C. Flowing *versus* Static Conditions for Measuring Multiple Exciton Generation in PbSe Quantum Dots. *J. Phys. Chem. C* **2010**, *114*, 17486–17500.
 39. Pijpers, J. J. H.; Ulbricht, R.; Tielrooij, K. J.; Osherov, A.; Golan, Y.; Delerue, C.; Allan, G.; Bonn, M. Assessment of Carrier-Multiplication Efficiency in Bulk PbSe and PbS. *Nat. Phys.* **2009**, *5*, 811–814.
 40. Beard, M. C.; Luther, J. M.; Semonin, O. E.; Nozik, A. J. Third Generation Photovoltaics based on Multiple Exciton Generation in Quantum Confined Semiconductors. *Acc. Chem. Res.* **2013**, *46*, 1252–1260.
 41. Allan, G.; Delerue, C. Role of Impact Ionization in Multiple Exciton Generation in PbSe Nanocrystals. *Phys. Rev. B: Condens. Matter Mater. Phys.* **2006**, *73*, 205423.
 42. Allan, G.; Delerue, C. Influence of Electronic Structure and Multiexciton Spectral Density on Multiple-Exciton Generation in Semiconductor Nanocrystals: Tight-binding Calculations. *Phys. Rev. B: Condens. Matter Mater. Phys.* **2008**, *77*, 125340.
 43. Velizhanin, K. A.; Piryatinski, A. Numerical Analysis of Carrier Multiplication Mechanisms in Nanocrystalline and Bulk Forms of PbSe and PbS. *Phys. Rev. B: Condens. Matter Mater. Phys.* **2012**, *86*, 165319.
 44. Delerue, C.; Allan, G.; Pijpers, J. J. H.; Bonn, M. Carrier Multiplication in Bulk and Nanocrystalline Semiconductors: Mechanism, Efficiency, and Interest for Solar Cells. *Phys. Rev. B: Condens. Matter Mater. Phys.* **2010**, *81*, 125306.
 45. Jorio, A.; Kasperczyk, M.; Clark, N.; Neu, E.; Maletinsky, P.; Vijayaraghavan, A.; Novotny, L. Optical-Phonon Resonances with Saddle-Point Excitons in Twisted-Bilayer Graphene. *Nano Lett.* **2014**, *14*, 5687–5692.